DEVELOPMENT AND EVALUATION OF A MUSCULOSKELETAL MODEL OF THE ELBOW JOINT COMPLEX

R.V. Gonzalez †, E.L. Hutchins ‡, R.E. Barr †, L.D. Abraham *

† Department of Mechanical Engineering, ‡ Biomedical Engineering Program,
* Department of Kinesiology and Health Education

The University of Texas at Austin
Austin, Texas 78712

Abstract -- *This paper describes the development and evaluation of a musculoskeletal model that represents human elbow flexion-extension and forearm pronation-supination. The length, velocity, and moment arm for each of the eight musculotendon actuators were based on skeletal anatomy and position. Musculotendon parameters were determined for each actuator and verified by comparing analytical torque-angle curves with experimental joint torque data. The parameters and skeletal geometry were also utilized in the musculoskeletal model for the analysis of ballistic elbow joint complex movements. The key objective was to develop a computational model, guided by parameterized optimal control, to investigate the relationship among patterns of muscle excitation, individual muscle forces, and movement kinematics. The model was verified using experimental kinematic, torque, and electromyographic data from volunteer subjects performing ballistic elbow joint complex movements.*

NOMENCLATURE

a(t)	Nominal muscle activation	p/s	Pronation-supination
u(t)	Neural signal	ANC	Anconeus
EMG	Electromyography	BIC	Biceps Brachii
EJC	Elbow joint complex	BRA	Brachialis
F^{MT}	Force of the musculotendon actuator	BRD	Brachioradialis
L^{MT}	Length of the musculotendon actuator	PRT	Pronator Teres
V^{MT}	Velocity of the musculotendon actuator	PRQ	Pronator Quadratus
MA	Moment arm (i.e. lever arm)	SUP	Supinator
f/e	Flexion-extension	TRI	Triceps Brachii

INTRODUCTION

The human EJC[1] is an intricate joint which produces combinations of movements that are unique within the human body and that are involved in performing many important tasks. It is partially responsible for the mobility of the hand, allowing the performance of duties which set humans apart from other mammals. The elbow joint's use in many daily activities makes it an important focus of biomechanics research.

[1] Elbow joint complex (EJC) refers to the articulations responsible for the combined movements of elbow flexion-extension, forearm pronation-supination, and forearm abduction-adduction (passive motion).

Biomechanical investigations of human movement have employed experimental, observational, and, more recently, computational modeling techniques [Anderson and Pandy, 1993]. The latter have provided both qualitative and quantitative insights into muscular control which are not always evident through observation or experimental procedures alone. Our objective was to use computational modeling techniques in investigating EJC movements. We used optimal control theory to solve the problem of muscular force indeterminacy caused by the redundant number of actuators present in the system.

Other models of the upper extremity have varied in their degree of complexity. They range from simple skeletal models without any muscle properties [An et al., 1984; Gonzalez et al., 1991] to models in which some muscle properties (i.e. force-length) are used in calculating muscle forces [An et al., 1989]. The latter study expressed the need for a detailed human elbow musculoskeletal model to investigate the dynamic characteristics of motor behavior about the EJC. Recently, optimal control was used to investigate planar shoulder movements with a mathematical musculotendon model similar to the one used in this study [Giat, 1990]. The computational model utilized in this study for the EJC goes beyond the scope of previous models by evaluating the EJC using three-dimensional kinematics, musculotendon dynamics, muscle excitations, optimal control, and experimental data to determine and verify musculotendon specific parameters.

METHODOLOGY

Experimental Methods

Experimental sessions of static EJC contractions were conducted to gather data needed to obtain musculotendon specific parameters and to calibrate and verify the model. The predictions obtained from the analytical model (both static and dynamic) were then compared to additional ballistic experimental data (EMG, kinematics, and joint torque).

Subjects

Seven healthy, male volunteer subjects, ages 27-45 years, were used for the static joint torque experiment. All subjects were right-hand dominant. One of these volunteers was further used for the ballistic EJC experiment.

Joint Torque Experiment

Isometric maximal joint torque data were collected on a LIDO™ active multi-joint testing unit. Using their dominant arm, subjects performed maximum voluntary contractions for three seconds at incremented angles over their entire range of motion while torque data were collected. A two-minute recovery period was allowed between contractions to avoid fatigue. The eight protocols implemented were elbow flexion with forearm supinated and forearm pronated, elbow extension with forearm supinated and forearm pronated, forearm supination with elbow extended and elbow flexed 90°, and forearm pronation with elbow extended and elbow flexed 90°. The experimental data for each subject were curve-fitted to a polynomial equation, and the curves were averaged across subjects for comparison with the analytical torque-angle results.

Ballistic Movement Experiment

Ballistic movements have been frequently studied for the elbow joint [e.g. Angel, 1974; Nahvi, 1989]. These studies have described EMG patterns of the agonist and antagonist muscles as tri-phasic. Tri-phasic muscle activation, which is depicted by the recorded EMG, is well documented and is a classic characteristic of ballistic movements. This pattern consists of three distinct phases. The first phase is the full activation of the agonist muscles preceding and during movement initiation. The second phase is the activation of the antagonist muscles to brake the moving segment. The third phase is the second activation of the agonist muscles to secure the final position. This pattern has been named ABC (A=Activation, B=Braking, C=Clamping) [Hannaford and Stark, 1985] and occurs in all ballistic movements which involve rapid movement initiation and an abrupt voluntary stop at a final specified position.

Ballistic movement patterns were executed for the dynamic data gathering session. The experimental protocols consisted of various combinations of ballistic elbow flexion, elbow extension, forearm pronation, and forearm supination. To demonstrate how the EJC model executes these movements, one ballistic protocol consisting of elbow flexion with forearm pronation is reported here. For this protocol, the subject was asked to start from a resting position with his humerus (upper arm) horizontal, supported, and strapped, and his forearm at approximately 10^{o} flexion and -50^{o} supination (p/s 0^{o} => neutral position, f/e 0^{o} => full extension). The arm was resting against a stop at the initial position to minimize baseline muscle activations. The subject was then asked to perform an elbow flexion with a simultaneous forearm pronation "as quickly as possible" without reaching the extreme positions of either motion. Since this movement required both ballistic initiation and voluntary braking, it showed a classic tri-phasic pattern for both f/e and p/s.

During the ballistic experimental sessions, EMG signals were gathered from eight muscles[2] (Figure 1) using five bi-polar surface electrodes and three fine wire intramuscular electrodes (BRA, BRD, and SUP muscles) and recorded using an Ariel™ Data Acquisition system sampling at 1000 Hertz. A digital bandpass filter [Barr and Chan, 1986] was applied to the digitized EMG data with frequency cut-offs at 20-200 Hz. This first processing step was used to remove unwanted noise produced by low frequency movement artifact or high frequency electrical noise that is uncharacteristic of the EMG signal. Following this process, full wave digital rectification was implemented and the signal was then normalized to its corresponding maximum value.

Position data of the forearm during elbow flexion and forearm pronation were obtained using a triaxial electrogoniometer similar to the one used in previous EJC investigations [Chao et al., 1980] and was sampled at 1000 Hz with the Ariel system. The kinematic raw data were also low-pass filtered [Lombrozo et al., 1988] using a digital filter at 3 Hz, then mapped from the voltage to the position (degrees) domain.

---

[2] Biceps Brachii, Brachialis, Brachioradialis, Triceps Brachii, Supinator, Pronator Teres, Anconeus, and Pronator Quadratus.

Modeling

The model represents elbow f/e and forearm p/s with eight musculotendon actuators crossing the joint. Ballistic EJC movements were modeled to describe the optimal kinematics, kinetics, musculotendon characteristics, and muscle excitations at the elbow joint. The elbow's f/e movement was modeled by a frictionless hinge joint rotation of the humerus and the ulna, with the center of rotation occurring at the center of the capitellum and trochlea [Chao et al., 1980]. Forearm p/s, which was considered to occur at the EJC, was modeled by frictionless rotation occurring about the forearm's system axis. This axis intersects the center of the anterior end of the radius and the center of the distal end of the ulna [Chao et al., 1980].

Musculotendinoskeletal Modeling

Computational musculotendinoskeletal models have been developed for the human lower extremity [Pandy et al., 1990] and upper extremity [Crowninshield, 1978; Giat, 1990; Yeo, 1976]. Recent models of musculoskeletal systems have used optimal control strategies to solve the indeterminate problem using a variety of performance indices [Flash, 1990]. These attempts have yielded a better understanding of the coordination of muscle forces and their corresponding electrical activities as determined by EMG. Incorporated within these latest musculoskeletal models [Giat, 1990; Pandy et al., 1990] has been a model of the musculotendon system. These musculotendon models have been developed to describe muscle and tendon function [Zajac and Gordon, 1989], so that more accurate actuator force predictions can be made.

The integrated components for developing computational musculoskeletal models have been established through recent efforts [Pandy et al., 1992; Pandy et al., 1990]. These components are illustrated in Figure 2 and include: (a) muscle excitation-contraction dynamics, (b) musculotendon dynamics, (c) skeletal dynamics, and (d) parameterized optimal control theory.

The corresponding dynamical equations for the EJC system can be written as follows:

(a) For muscle excitation-contraction,

$$\dot{a} = (1/\tau_{rise})(u_i - a_i)u_i + (1/\tau_{fall})[u_i - (a_i - a_{min}) - (u_i - a_i)u_i] \quad i=1,8 \qquad (1)$$

where u_i is the input excitation given to the i^{th} muscle in the model; a_i is the level of activation in the i^{th} muscle; τ_{rise} and τ_{fall} are the rise and decay times for muscle activation, respectively.

(b) For musculotendon dynamics,

$$\dot{F}_i^{MT} = f_i(\underline{q}, \dot{\underline{q}}, F_i^{MT}, a_i); \qquad i=1,8 \tag{2}$$

where F_i^{MT} is an 8x1 vector of musculotendon actuator forces; $\underline{q}, \dot{\underline{q}}, \ddot{\underline{q}}$ are 2x1 vectors of body segmental displacements, velocities, and accelerations.

(c) For skeletal dynamics

$$A(\underline{q})\ddot{\underline{q}} = B(\underline{q})\dot{\underline{q}}^2 + C(\underline{q}) + M(\underline{q})F^{MT} \tag{3}$$

where $A(\underline{q})$ is the 2x2 system mass matrix; $B(\underline{q})\dot{\underline{q}}^2$ is a 2x1 vector describing both Coriolis and centrifugal effects; $C(\underline{q})$ is a 2x1 vector containing only gravitational terms; $M(\underline{q})$ is a 2x8 MA matrix (see Skeletal Geometry).

Existing computer algorithms for modeling the mechanical response of the musculotendon system were used with the following parameters for the eight actuators: resting muscle fiber length, maximum isometric force, tendon slack length, and pennation angle (see Pandy et al., 1990, for details). The values for the parameters were based on solutions determined in the model using the isometric experimental results (see Results). Included in the larger dynamic model were the calculations of musculotendon length and velocity, and their corresponding moment arms [Hutchins et al., 1993]. Since the state equations [(1), (2), (3)] of the musculotendinoskeletal system were represented as first order ordinary differential equations, a numerical Runge-Kutta routine [Brankin, 1992] was used to integrate all the states of the model (time rate of change of: muscle force, muscle activation, position, and velocity).

Skeletal Geometry

Constant, discrete origin and insertion points were defined from the attachment locations of the muscles and tendons on the bone [Yamaguchi et al., 1990]. Each point was defined with respect one of the three reference frames (humerus, ulna, or radius) on which it was located. The points at which these muscles contacted a bone other than the attachment sites were designated as "effector

points". These effector points were in some cases dependent on both the f/e and p/s joint angles, representing deviations of the muscle line of action from a straight line connecting the origin and insertion.

The L^{MT} was calculated as the magnitude of the vector connecting the origin and insertion points. In cases where effector points were necessary to describe the muscle path (BIC, SUP, PRT, and ANC), L^{MT} was the sum of the line segments connecting the points. Since the insertion point was defined by a different segment reference frame than the origin point, the insertion coordinates were transformed to the origin reference frame for this calculation using:

$$L^{MT} = |origin - Transformation * insertion| \tag{4}$$

The transformation matrix was dependent on the type of joint the actuator crossed. The elbow was modeled using rotation angles for f/e, p/s, and the carrying angle (abduction-adduction). The translations were based on anthropometric data for the upper extremity bones [Seireg and Arvikar, 1989]. In describing the muscle path for the BIC and SUP actuators, an additional assumption was made to describe the wrapping around the radius that occurs when the muscles contract. An appropriate supination arc length was added to the sum of the line segments. The velocity of the musculotendon actuator (V^{MT}) was the magnitude of the analytical time rate derivative of L^{MT}.

The moment arm which was needed to convert musculotendon force to moment about a joint was determined by the magnitude of the cross product of the unit vector from the origin to the insertion point and a vector joining the origin point to the joint center using:

$$MA = \frac{|\vec{OI} \times \vec{OJ}|}{|\vec{OI}|} \tag{5}$$

where: $\vec{OI}$ was the vector for the musculotendon origin to insertion point.

$\vec{OJ}$ was the vector from the musculotendon origin to the respective joint center.

In the cases where effector points were present, they were substituted appropriately into equation (5) (see Hutchins, 1993 for details). Because anatomical moment arms were scarce in the

literature, especially for the muscles in the forearm, the calculated analytical moment arms based on equation (5) were not altered in any way.

Parameter Determination

Torque-angle relationships are dependent on the interaction of the isometric force and moment arm of each musculotendon actuator which spans the joint. Both components are generated as a function of joint position. Musculotendon isometric force is dependent on the optimal muscle fiber length, peak isometric force, pennation angle, and tendon slack length. The pennation angle was determined by investigating a variety of literature sources for the most consistent measurement. Initial values for optimal fiber length and physiological cross-sectional area were gathered from cadaver studies reported in the literature [Amis et al., 1979; An et al., 1981; Giat, 1990]. The joint angle where a musculotendon's peak force occurs is controlled by the optimal (resting) fiber length and the tendon slack length. Adjustments in these values cause horizontal shifts in the force-length curve and, therefore, the torque. Modifications were made to the initial parameter values to attempt to maintain a normalized muscle length between 0.5 and 1.5 over the entire range of motion. Vertical adjustments were also made by varying the peak isometric force of the individual muscles while keeping them within the proportion of their typical physiological cross-sectional area.

Muscle torque was computed as the moment arm times the muscle force. The torque of all muscles assumed to participate in a specific motion was summed for each joint position to form the total torque curve for that motion. The goal was to scale, by adjusting the parameters, the eight analytical torque-angle relationships to correspond to the experimental torque-angle relationships. The most accurate parameter values were decided once an estimated (root mean square error) best-fit was made for the curves.

Optimal Control

The mechanical redundancy posed by the numerous actuators, even when only considering two degrees-of-freedom, required that this problem be solved using a non-classical method. A

numerical optimal control package [Powell, 1978] was used to converge on minimum time sub-optimal solutions of an elbow flexion and forearm pronation movement starting from rest and ending at rest (i.e. zero velocity and zero acceleration) (see Pandy et al., 1992, for details).

For this minimum time movement, the performance criteria and constraints were therefore:

$$J = min \int_{t_0}^{t_f} dt$$

under the conditions:

$$q_{t_f} = q_{spec}, \dot{q}_{t_f} = \dot{q}_{spec}, \ddot{q}_{t_f} = \ddot{q}_{spec} \quad \text{and}$$

$$0 \le u_i \le 1; \quad i=1,8 \qquad (6)$$

Initial states (t=0) were optimized by minimizing the square root of the sum of the stresses in each muscle at the initial pre-specified arm position under the constraints of zero velocity and zero acceleration and that the activation of each muscle be within 20% of any member of its synergistic group.

Computational Facilities

All computational work was done on either a Silicon Graphics Workstation (IRIS Indigo, XS24) or an IBM RS/6000. The operating systems were IRIX 4.0.5F and AIX 3.2, with FORTAN compiler versions F77 3.4.1 and XLF 2.03 for the IRIS and RS/6000, respectively.

RESULTS AND DISCUSSION

Parameter Determination

Table 1 displays the final values of each parameter for each actuator determined in the static experiment, which were then applied to the dynamic optimization. Experimental values from cadaver studies are available for comparison; however, these data are limited in their usefulness. Cadaver specimens have undergone some physiological changes that affect measurements, and tendon slack length cannot be actually measured. Optimal fiber length values reported in literature

are slightly smaller (0.002 - 0.02 m) than the analytical values, except for the supinator. Optimal fiber lengths for the SUP were reported between 0.033 m and 0.047 m [Amis, et al., 1979; An, et al., 1981].

The physiological cross-sectional area (PCA) of a muscle was assumed to be proportional to a muscle's peak isometric force (F_m^o). Therefore, to properly scale F_m^o, they were adjusted using this proportionality criteria to match the net isometric joint torques. As a result, the F_m^o parameter values calculated were greater than the theoretical F_m^o as calculated from the literature values of PCA times the specific tension of a muscle (16-30 $N\text{-}cm^{-2}$) [McDonagh and Davies, 1984]. This outcome was due to much older and predictably weaker cadaver specimens when compared to the subjects used in this study.

The analytical moment arms calculated with equation (5) were compared to published data when possible. Elbow flexor moment arms predicted by the model compared favorably with both the trends and magnitudes reported in literature [Amis, et al., 1979; An, et al., 1981]. The model gave ranges of 15-28 millimeters (mm) for the BRA, 20-32 mm for the BIC, 18-35 mm for the BRD, and 10-20 mm for the PRT. Moment arm-angle relationships peaked around 100^o flexion. The moment arm-angle relationships for the elbow extensors ranged from 12-29 mm for the TRI and 6-12 mm for the ANC which agrees with published values ranging from 16-24 mm and 6-10 mm, respectively [Amis, et al., 1979]. For the forearm supinators, the moment arms for the BIC and SUP appeared relatively constant. This effect was caused by the actuator wrapping around the bone producing a moment arm equivalent to the radius of the radial head. The values were within the small range (BIC: 10-12 mm, SUP: 7-13 mm) presented in the literature [Caldwell, 1987].

Table 1 - Musculotendon Parameters for the Actuators in the EJC Musculoskeletal Model.

Actuator	Resting muscle fiber length (m)	Peak muscle force (N)	Tendon slack length (m)	Pennation angle (deg)
Biceps Brachii	0.14	670	0.20	2.5
Brachialis	0.07	720	0.043	4
Brachioradialis	0.144	430	0.12	4
Triceps Brachii	0.10	1750	0.175	15
Supinator	0.102	320	0.01	0
Pronator Teres	0.07	390	0.085	9.6
Pronator Quadratus	0.036	370	0.008	9.9
Anconeus	0.045	450	0.013	0

Torque-angle relationships

Figure 3 shows the analytical torques produced by the flexors at full supination, after all the modifications to the parameters were performed, compared with the experimental flexion torque. Similarly, results of the torques produced by the pronators are shown in Figure 4. The discontinuities in the pronator curves are a result of the muscles' pronation torque going to zero at the neutral forearm position (i.e. pronation moment arm becomes a supination moment arm).

Ballistic Computational Solution

Results of the ballistic computational solution were compared to the ballistic experimental kinematic and EMG data. Figure 5 shows both the predicted (modeled) and experimentally measured positions of a ballistic elbow flexion and forearm pronation. The predicted trajectory of the p/s angle showed that it slightly overshot the final position but then recovered to meet the final constraints. Such overshooting has been described in experimental and modeling reports when

speed is more heavily favored than the end point accuracy. The final time difference between the model's solution and experiment was 12 milliseconds.

This comparison (Figure 5) indicates an extremely good fit between what the subject performed and what the model concluded was the minimum time solution. The solution for f/e is almost exactly what the subject performed. The slight variation between the p/s trajectories indicates that the model was much more sensitive to changes in the activity and parameter estimation of the muscles that contributed to p/s. This sensitivity is due to the complexity of the actuators (BRD, PRT, PRQ) that are strictly along the forearm (i.e. muscles wrapping around bone and estimation of the MA based on the system axis of p/s). Nonetheless, given this complexity of the skeletal geometry of the forearm muscles, the p/s predicted trajectory is very close to the subject's experimental motion.

Predicted individual musculotendon forces for the eight muscles were analyzed to determine their time-varying contribution to the ballistic movement. Figure 6 shows that the primary flexors' (BIC, BRA, BRD) force magnitudes all increased and peaked at about 0.1 second into the movement. After this point, the force magnitude decreased (resulting from a lower flexor activity, Figure 9) to allow the arm to decelerate. The BIC and BRD then reactivated to clamp the final position (also indicated in Figure 9). The reactivation of these muscles, as opposed to no reactivation of the BRA, showed that the torque produced by these actuators was also used to assist in clamping the forearm movement. The extensor time-varying forces (TRI and ANC, Figure 7) show how these extensor muscles acted to slow the movement and to meet the final kinematic constraints. The model predicted the same pattern of force generation for both extensors, with the TRI showing significantly greater magnitude. The forearm muscles that contribute to the p/s movement (Figure 8) all initially increased in magnitude. After the initial peak (t=0.05) the SUP decreased throughout the remainder of the movement. This initial SUP activity occurred to counter the passive forces caused by the elastic tissues in the BRD muscle. The PRT and PRQ musculotendon force initially increased during the movement and also near the final time to secure the p/s angle and balance the supination produced by the BIC and BRD.

The predicted activations from the model's sub-optimal minimum time solution were compared to the experimental activations (i.e. processed EMG). The BIC, BRA and BRD (Figure 9) showed a full initial activation ending between the range of 0.1 - 0.2 seconds into the movement. The model's solution not only indicated the magnitude of the activity for the flexor muscles, but also the amount of time the muscles were active as compared to the EMG. A secondary burst close to the final time was also shown for the BIC and BRD to brake the elbow flexion and forearm pronation. The PRT and PRQ model activations varied throughout the movement to produce pronation and was a pattern generally observed in the measured EMG. These flexor and pronator activation results corresponded with what is expected in ballistic movements (tri-phasic pattern; A and C). The predicted activation and force in the TRI and ANC showed the classic second burst of activity to brake the elbow's flexion and the TRI compared nicely with the measured EMG. However, the predicted activation of the ANC muscle's did not represent the initial activity shown in the experimental EMG because the ANC muscle is believed to contribute to the stabilization of the EJC (Caldwell, 1987). This stabilization was not accounted for in the EJC model.

The predicted SUP muscle activity showed initial activity lasting about 0.05 seconds and then remained silent for the remainder of the movement. Although it appears to contradict the experimental EMG measurement, one must note that the SUP EMG activity was taken with fine wire electrodes and if the muscle was fully activated, the frequency component would be much higher than the activity of the other muscles taken with surface electrodes. The magnitude of the processed SUP EMG signal was high because it was normalized to its respective maximum. Therefore, given this type of normalization procedure, small amounts of muscle activity appear much larger than is actually the case. Although this type of normalization at times misrepresents the overall magnitude of the EMG signal, it was difficult to establish a "maximum" EMG normalization value based on either maximum voluntary isometric contractions (i.e. the wire electrodes can cause pain and present some risks) or with a dynamic maximum value determined across all the protocols for each muscle.

In general, the model predicted muscle excitation patterns similar to the processed EMGs. The variations between the computed and experimental muscle activations are attributed, in part, to the processing of the raw EMG data and the manner in which neural to muscle activation is modeled (muscle excitation-contraction dynamics). Overall, the presence of the tri-phasic activation pattern in the model's solution, especially for f/e, and the reasonably good comparison with experimental measurements (i.e. kinematics and muscle activity) validates the model and thus gives credence to the time-varying muscle force predictions. Additionally, the difference between the predicted and experimental movement time of 12 milliseconds (< 4% difference) signifies that the musculotendinoskeletal model of the EJC represented well the capabilities of this joint while performing ballistic movements.

CONCLUSIONS

The parameters determined in this study (Table 1) appear to be relatively accurate, based both on comparison with related work done by others and on their successful application to a modeled ballistic EJC movement (simultaneous ballistic elbow flexion and forearm pronation). These results suggest that the parameters determined are reliable for computational musculoskeletal models such as the one presented here. Of particular significance is the determination of the tendon slack length of each muscle, which is a parameter not easily measured even in cadaver specimens. The results of this attempt to model the EJC in ballistic movements provide a good comparison between kinematic data, and a favorable comparison between experimental and predicted muscle activations. Additionally, results of the musculotendon forces (Figures 6-8), indicate that it would be incorrect to assume synergistic muscles produce similar time-varying forces. Therefore, to lump these muscles together to reduce the redundancy of the system would be erroneous.

This EJC model can also be used in forward integration kinematic solutions by using processed experimental measurements of muscle activation (EMG) to drive the model. The attempt to use

processed EMG to obtain accurate joint torque and kinematic solutions has been promoted by other authors as well [Hof, 1987; White and Winter, 1986]. It is proposed that the representation of muscle activation can be obtained from the EMG by using a processing scheme which maps the EMG signal to what the model uses as the overall muscle activation signal. Such an attempt by our group was recently shown to be feasible in determining the torque for the elbow joint by using neural network theory in conjunction with classical signal processing schemes [Lester et al., 1994].

Acknowledgments

The authors wish to thank Marcus Pandy, Jim Ziegler, and Frank Anderson for the musculotendon computer algorithm and for guidance during this project. This research was supported in part by NASA/JSC, Grants NGT-70252 and NAG9-588.

REFERENCES

Amis, A.A., Dowson, D., and Wright, V. (1979) Muscle strength and musculo-skeletal geometry of the upper limb. *Engng. Med.* **8**:41-48.

An, K.N., Hui, F.C., Morrey, B.F., Linscheid, R.L., and Chao, E.Y. (1981) Muscles across the elbow joint: A biomechanical analysis. *J. Biomechanics* **14**:659-669.

An, K.N., Kaufman, K.R., and Chao, E.Y.S. (1989) Physiological considerations of muscle force through the elbow joint. *J. Biomechanics* **22**:1249-1256.

An, K.N., Kwak, B.J., Chao, E.Y., and Morrey, B.F. (1984) Determination of muscle and joint forces: a new technique to solve the indeterminate problem. *J. Biomed. Engng.* **106**:364-367.

Anderson, F.C. and Pandy, M.G. (1993) Storage and utilization of elastic strain energy during jumping. *J. Biomechanics* **26**:1413-1428.

Angel, R.W. (1974) Electromyography during voluntary movement: The two burst pattern. *Electroenceph. and Clin. Neurophysiology* **36**:493-498.

Barr, R.E. and Chan, E.K.Y. (1986) Design and implementation of digital filters for biomedical signal processing. *J. Electrophysiol. Tech.* **13**:73-93.

Brankin, R.W., Gladwell, I., and Shampine, L.F. (1992) RKSUITE: a suite of Runge-Kutta codes for the initial value problem for ODEs. Softreport 92-S1, Department of Mathematics, Southern Methodist University, Dallas, Texas.

Caldwell, G.E. (1987) *Applied Muscle Models in Prediction of Forces of the Elbow*. PhD Dissertation, Simon Fraser University.

Chao, E.Y., An, K.N., Askew, L.J., and Morrey, B.F. (1980) Electrogoniometer for the measurement of human elbow joint rotation. *ASME J. Biomechanical Engineering* **102**:301-310.

Crowninshield, R.D. (1978) Use of optimization techniques to predict muscle forces. *ASME J. Biomechanical Engineering*, pp. 88-92.

Flash, T. (1990) Organization of human arm movement control. Winters, J.M. and Woo, S.L-Y. (eds.): *Multiple Muscle Systems: Biomechanics and Movement Organization*, Springer-Verlag, New York, pp. 282-301.

Giat, Y. (1990) *Prediction of Muscular Synergism and Antagonism of Human Upper Extremity -- A Dynamic Optimization Approach*. PhD Dissertation, Univ. of Maryland.

Gonzalez, R., Micallef, D., Barr, R., and Abraham, L. (1991) Prediction of muscle force patterns in elbow flexion / extension using mathematical modeling and electromyography. *Proc. of the 10th Southern Biomed. Eng. Conf.*, Atlanta, Georgia, pp. 182-185.

Hannaford, B., and Stark, L. (1985) Roles of the elements of the triphasic control signal. *Experimental Neurology* **90**:619-634.

Hof, A.L., Pronk, C.N.A., van Best, J.A. (1987) Comparison between EMG to force processing and kinetic analysis for the calf muscle moment in walking and stepping. *J. Biomechanics* **20**(2):167-178.

Hutchins, E.L. (1993) *The Musculoskeletal Geometry of the Human Elbow and Wrist: An Analysis Using Torque-Angle Relationships*. Masters Thesis, University of Texas at Austin.

Hutchins, E.L., Gonzalez, R.V., and Barr, R.E. (1993) Comparison of experimental and analytical torque-angle relationships of the human elbow joint complex. *Proc. of the 30th Ann. Rocky Mtn. Bioeng. Symp.*, San Antonio, Texas, pp. 17-24.

Lester, W.T., Fernandez, B., Gonzalez, R.V., and Barr, R.E. (1994) A neural network Approach to electromyographic signal processing for a motor control task. *Proc. of the 1994 American Control Conference*, Baltimore, Maryland, June, 1994. (in press)

Lombrozo, P.C., Barr, R.E., and Abraham, L.D. (1988) Smoothing of noisy human motion data using digital filtering and spline curves. *Proc. of IEEE Eng. in Med. & Biol. Soc. Conf.*, New Orleans, Louisiana, pp. 653-654

McDonagh, M.J.N. and Davies, C.T.M. (1984) Adaptive response of mammalian skeletal muscle to exercise with high loads. *European J. of Appl. Physio.*, 52:139-155.

Nahvi, M. (1989) Fast movements of human arm: Reflections on control issues. *Proc. of the IEEE Inter. Conf. on Sys., Man and Cyb.* Cambridge, Massachusetts. 3:1109-1112.

Pandy, M.G., Anderson, F.C., and Hull, D.G. (1992) A parameter optimization approach for the optimal control of large-scale, musculoskeletal systems. *ASME J. Biomechanical Engineering*. **114**(4):450-459.

Pandy, M.G., Zajac, F.E., Sim, E., and Levine, W.S. (1990) An optimal control model for maximum-height human jumping. *J. Biomechanics* **23**(12):1185-1198.

Powell, M.J.D. (1978) A fast algorithm for nonlinearly constrained optimization calculations. Matson, G.A. (ed.): *Numerical Analysis: Lecture Notes in Mathematics*. Springer-Verlag, 630:144-157.

Seireg, A., and Arvikar, R. (1989) *Biomechanical Analysis of the Musculoskeletal Structure for Medicine and Sports*. Hemisphere Publishing Corp. New York, NY.

White, S.C., and Winter, D.A. (1986) The prediction of muscle forces using EMG and a muscle model. *North American Congress of Biomechanics I (NACOB)*, pp. 67-68.

Yamaguchi, G.T., Sawa, A.G.U., Moran, D.W., Fesler, M.J., and Winter, J.M. (1990) A survey of human musculotendon actuator properties. Winters, J.M. and Woo, S.L-Y. (eds.): *Multiple Muscle Systems: Biomechanics and Movement Organization*. Springer-Verlag, New York, pp.713-773.

Yeo, B.P. (1976) Investigations concerning the principle of minimal total muscular force. *J. Biomechanics* 9:413-416.

Zajac, F.E., and Gordon, M.E. (1989) Determining muscle's force and action in multi-articular movements. *Exercise and Sport Science Review* **17**:187-230.

Figure 1. Schematic representation of the musculoskeletal model used to simulate ballistic EJC movements. The skeleton was modeled as a two segment, two-degree-of-freedom system, where the f/e axis was a simple revolute joint and the p/s axis oriented from the proximal end of the radius to the distal end of the ulna. All joints were considered frictionless. A total of eight musculotendinous units actuated the model. The two heads of the BIC and the three heads of the TRI were each modeled as one actuator. Actuators which contributed to elbow flexion were BIC, BRA, BRD, and PRT. Actuators which contributed to elbow extension were TRI and ANC. Actuators which contributed to forearm pronation were PRT, PRQ, and BRD. Actuators which contributed to forearm supination were SUP and BRD. The BRD musculotendon contributed to either forearm pronation or forearm supination based on the instantaneous orientation of the forearm.

Figure 2. The three components of the musculotendinoskeletal model represent muscle excitation-contraction dynamics, musculotendon dynamics, and skeletal dynamics. These components are the basis for the musculotendinoskeletal model. This model is then combined with an optimal control algorithm to determine the minimum time solution for f/e and p/s movements, which are compared to experimental results.

Figure 3. Torque-angle relationships for the elbow flexors are: total modeled (bold solid), Experimental (bold dashed), BIC (solid), BRA (dotted), BRD (dot-dashed), and PRT (dashed). Zero degrees is full elbow extension. The forearm is supinated. $\mathcal{E}$ = 0.136 is the root mean square error between the experimental and total modeled data.

Figure 4. Torque-angle relationships for the forearm pronators with the elbow extended are: total modeled (bold solid), Experimental (bold dashed), PRT (solid), BRD (dashed), and PRQ (dotted). The BRD and PQ torques become inactive at the neutral position, which is 0° on the graph. Negative angle was in the supination direction. The elbow was extended. $\mathcal{E} = 0.143$ is the root mean square error between the experimental and total modeled data.

Figure 5. Experimental and model predicted (bold lines) position trajectories are shown for elbow f/e and p/s. Zero degrees was full elbow extension and neutral forearm position. Negative angles were for supinated forearm positions.

Figure 6. Predicted musculotendon force of primary flexors during a ballistic flexion and pronation are shown for BIC (solid), BRA (short dash), and BRD (long dash).

Figure 7. Predicted musculotendon force of primary extensors during a ballistic flexion and pronation are shown for TRI (dashed) and ANC (solid).

Figure 8. Predicted musculotendon force of primary pronators and supinators during a ballistic flexion and pronation are shown for SUP (solid), PRT (short dash), and PRQ (long dash).

Figure 9. Musculotendon activation is shown for bandpassed rectified normalized EMG (light line) and nominal muscle activation used by the model (heavy line).

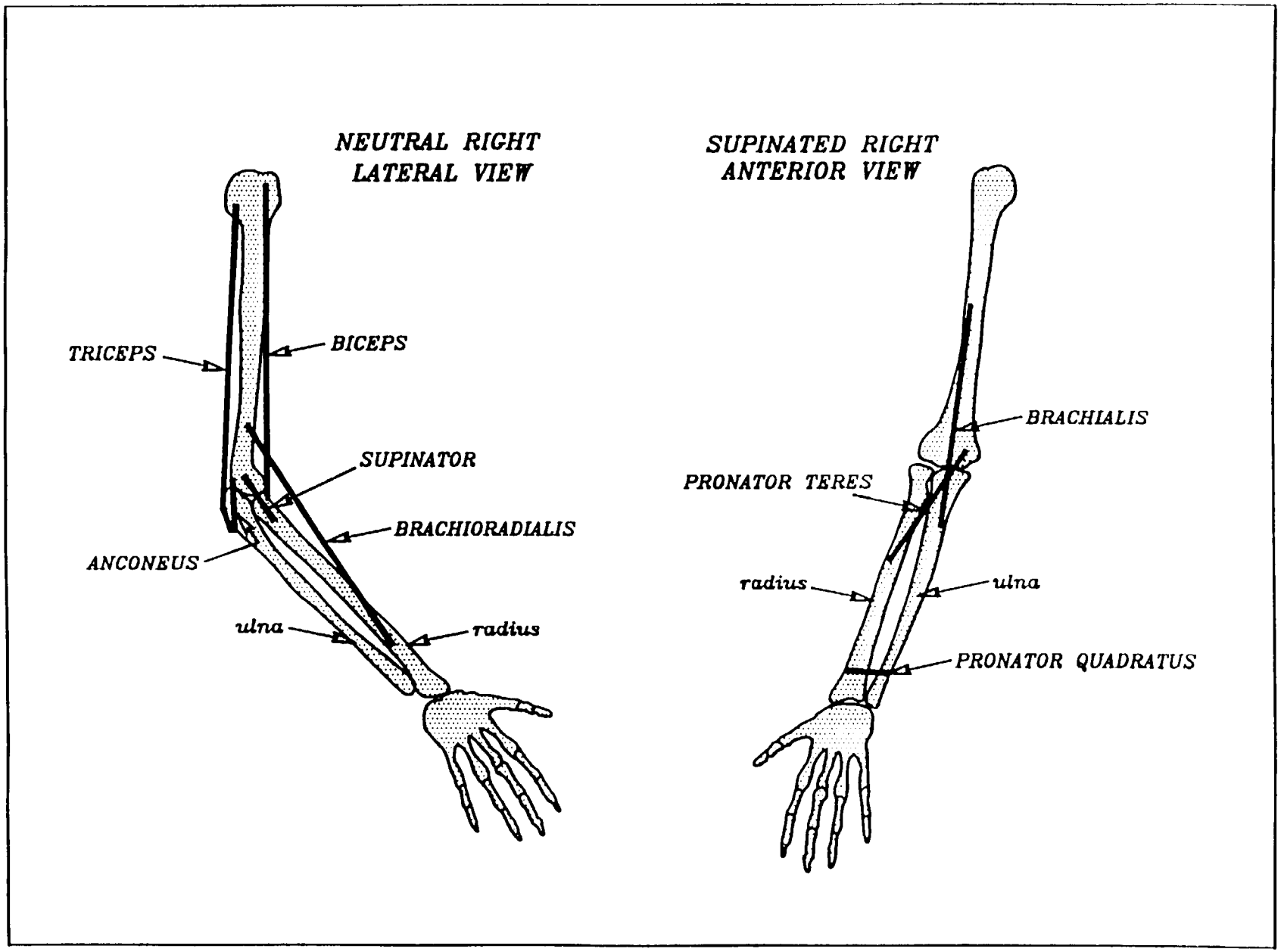
NEUTRAL RIGHT
LATERAL VIEW
TRICEPS
BICEPS
SUPINATOR
BRACHIORADIALIS
ANCONEUS
ulna
radius
SUPINATED RIGHT
ANTERIOR VIEW
BRACHIALIS
PRONATOR TERES
radius
ulna
PRONATOR QUADRATUS

Figure 1

Figure 2.
Gonzalez, R.V., et al.

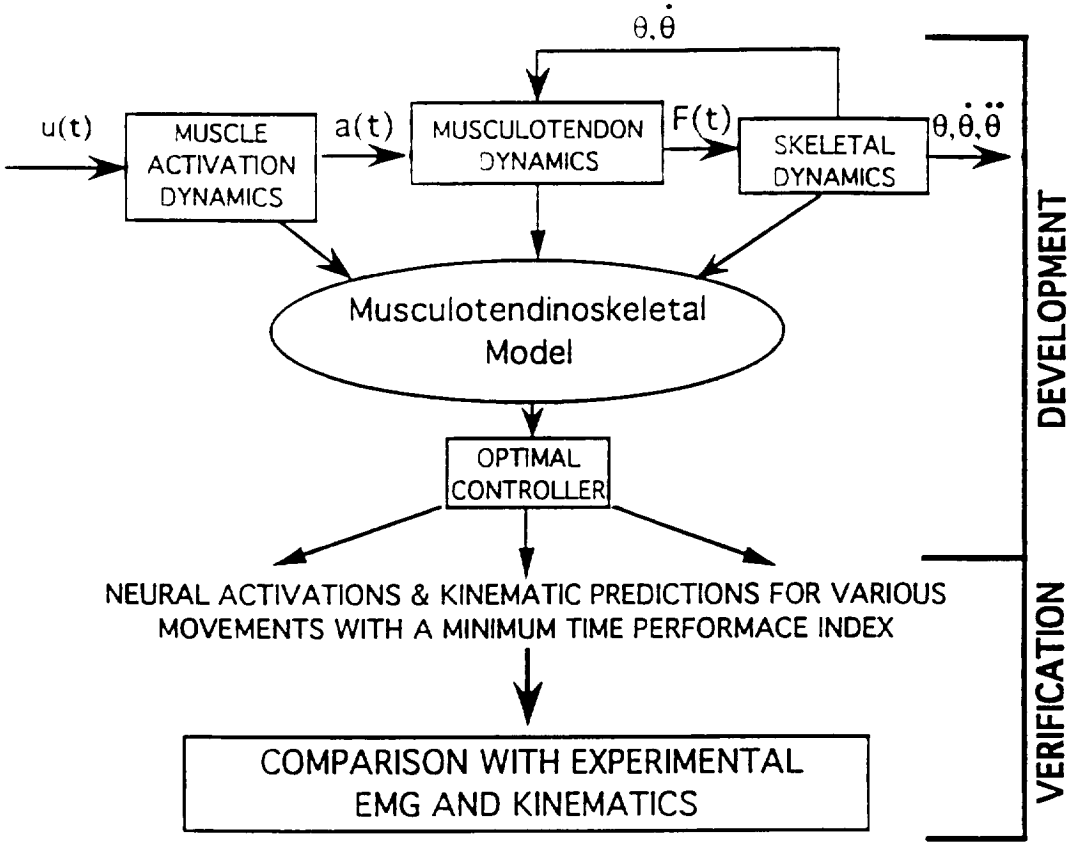

Figure 3
Gonzalez, R.V., et al.

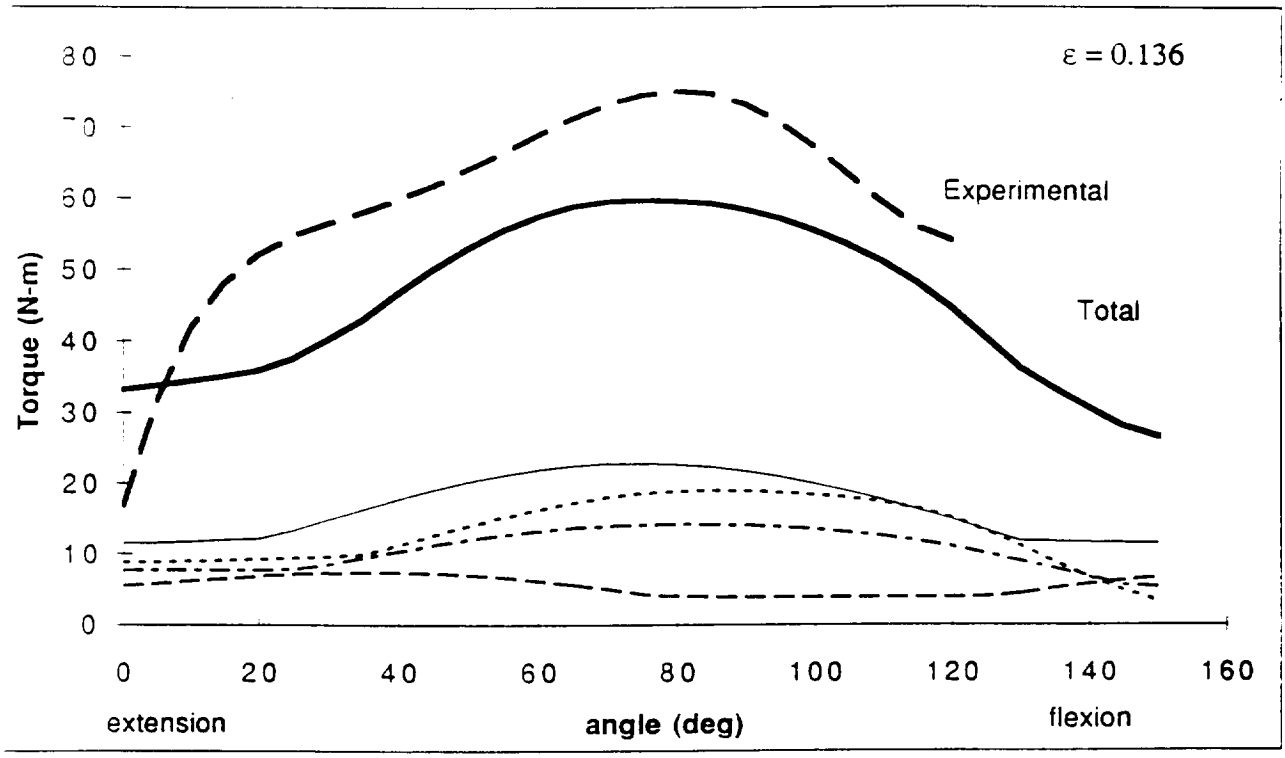

Figure 4
Gonzalez, R.V., et. al.

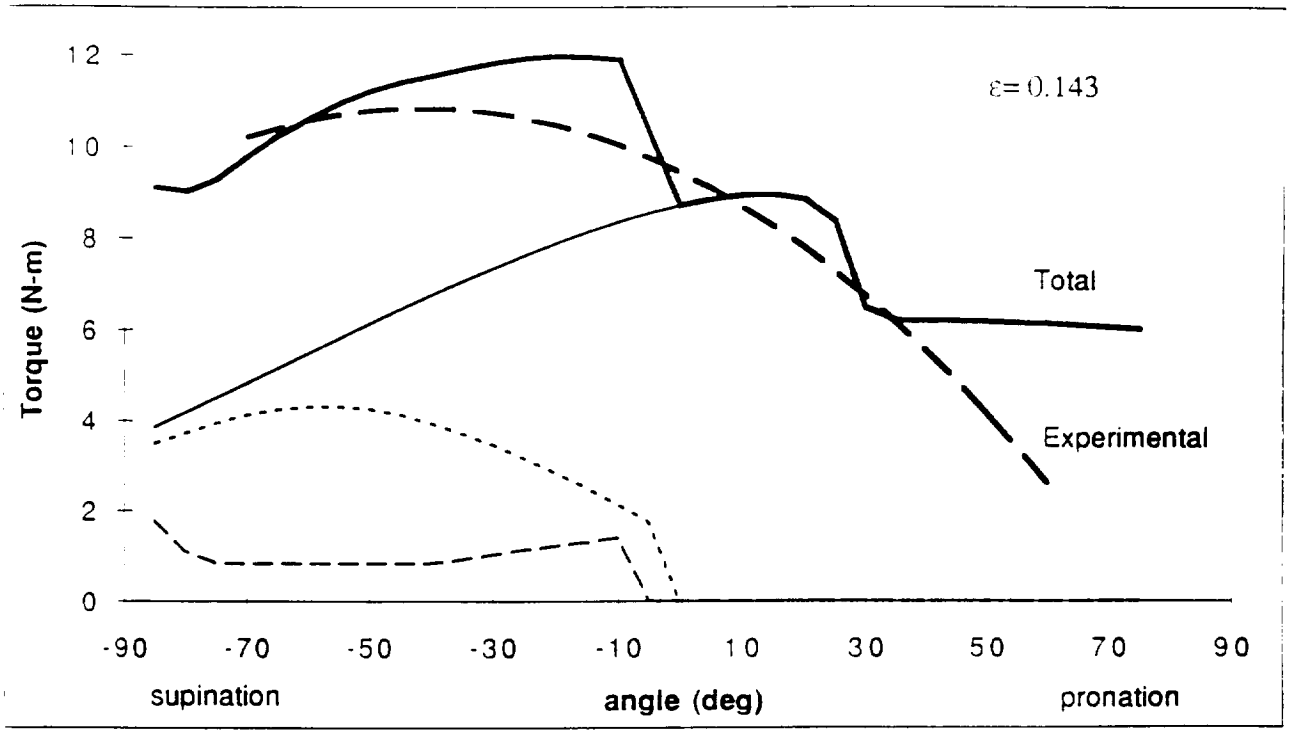

Figure 5
Gonzalez, R.V..

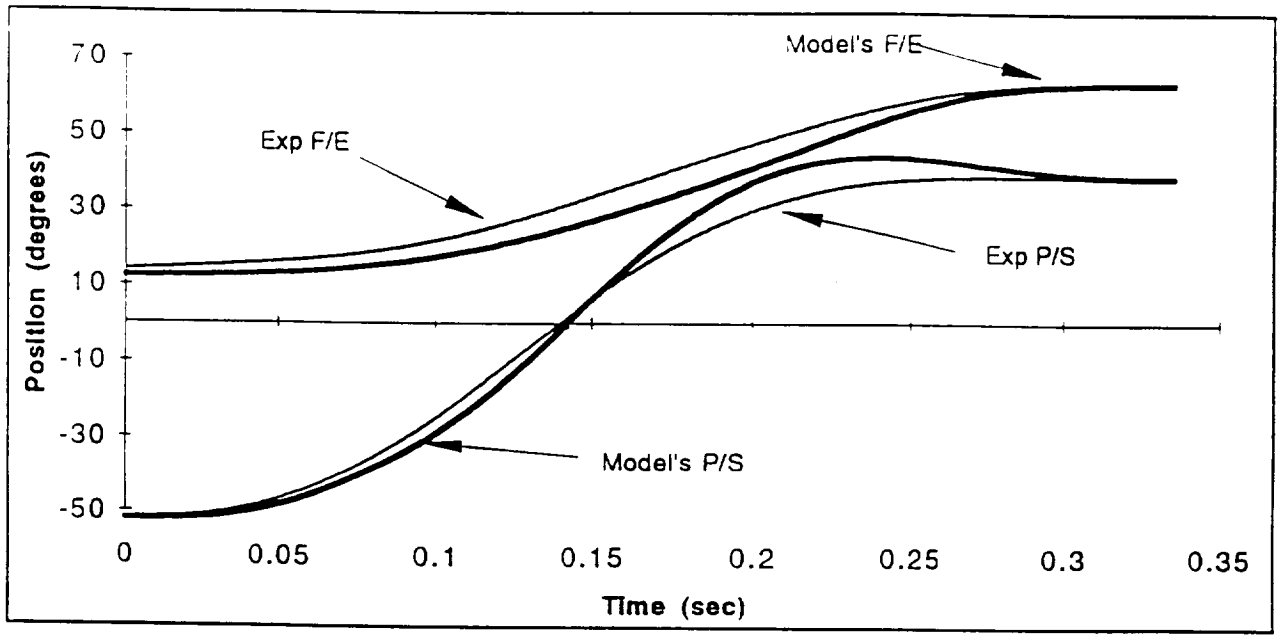

Figure 6
Gonzalez, R.V.,

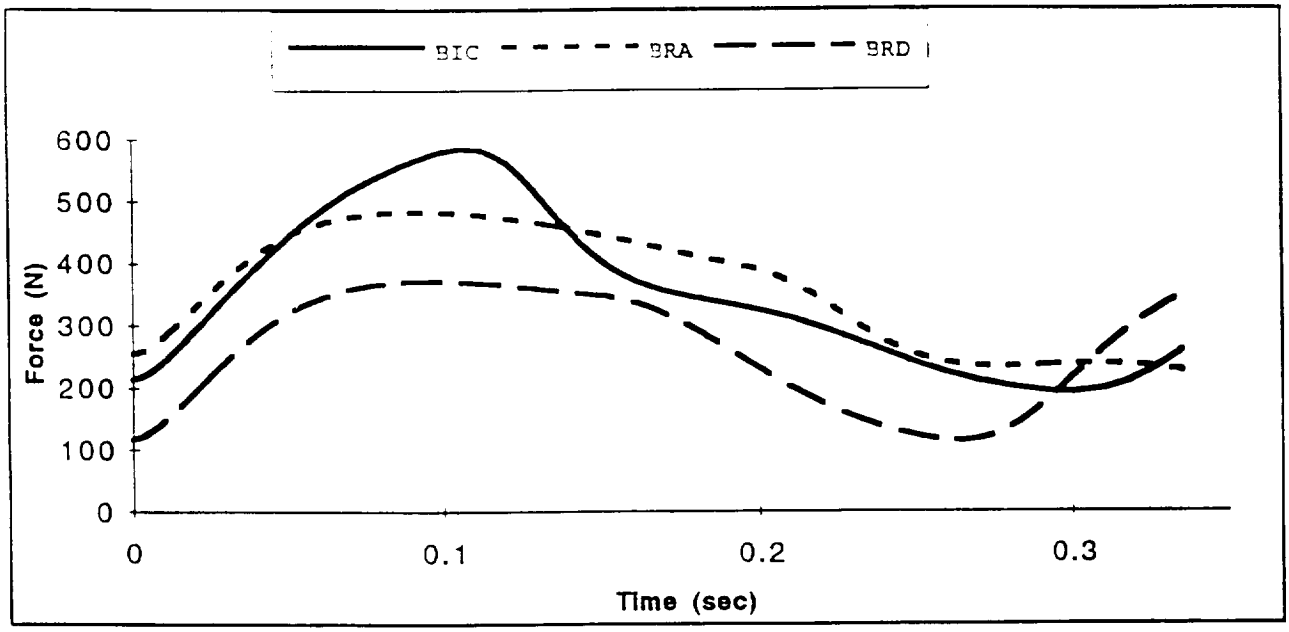

Figure 7
Gonzalez, R.V., et

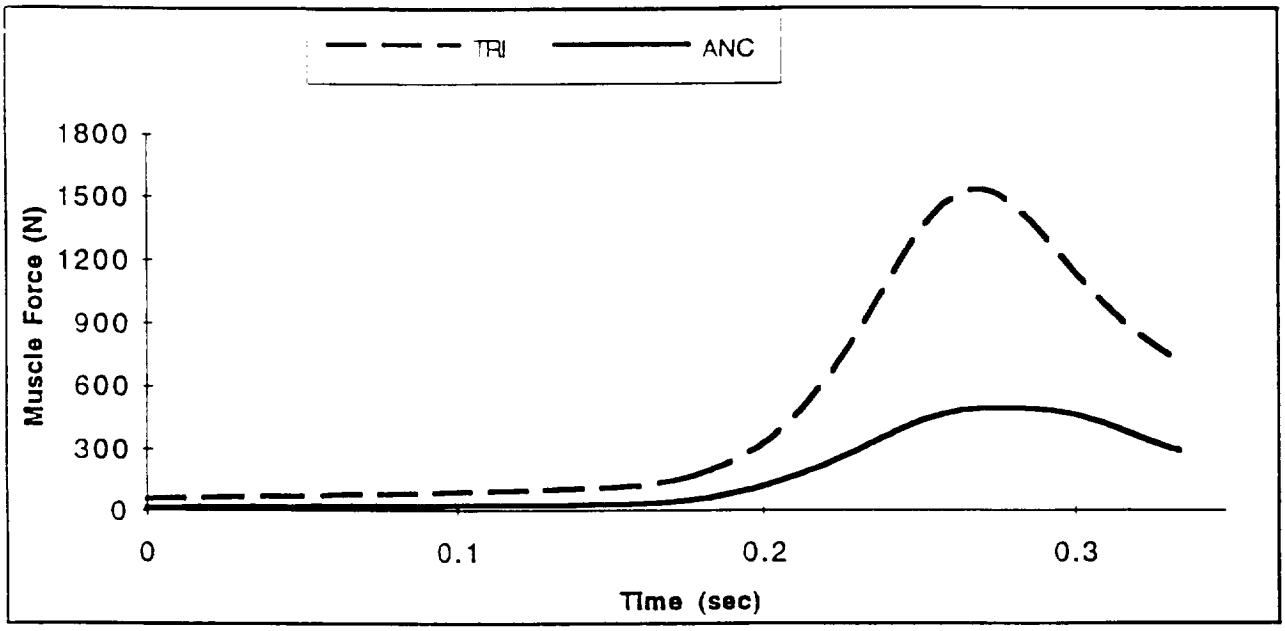

Figure 8

Gonzalez, R.V., et al.

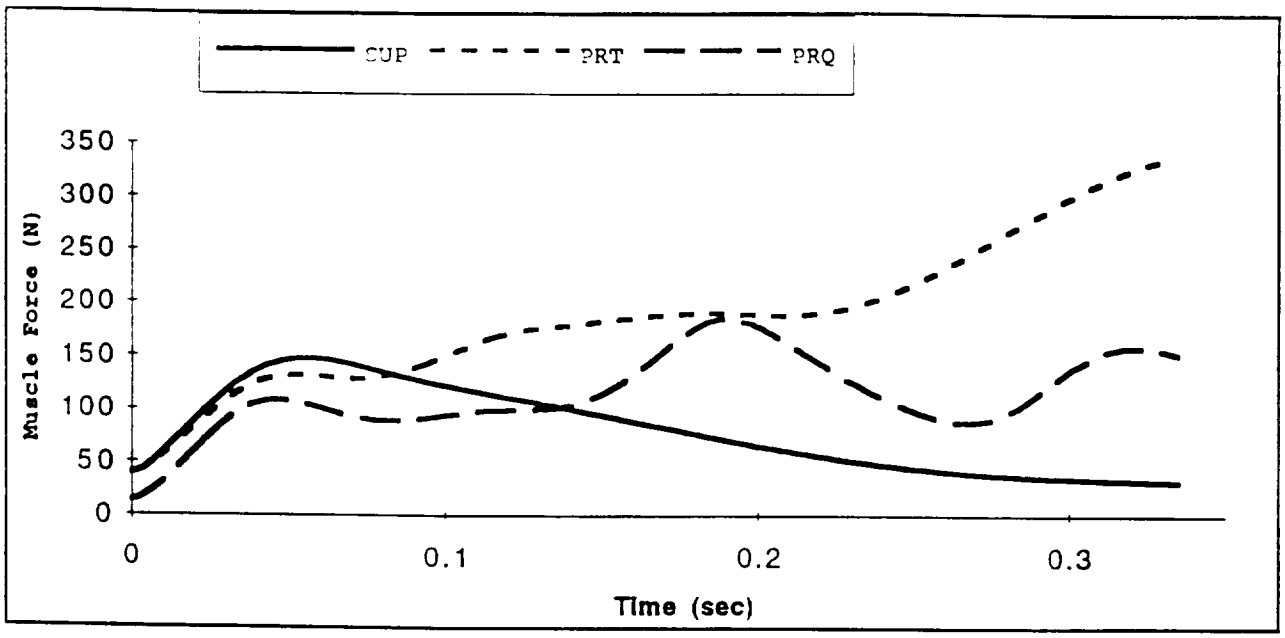

Figure 9

Gonzalez, R.V., et al.